Deep mantle structure as a reference frame for movements in and on the Earth

Trond H. Torsvik[a,b,c,d,1], Rob van der Voo[b,e], Pavel V. Doubrovine[a,b], Kevin Burke[b,d,f], Bernhard Steinberger[a,b,g], Lewis D. Ashwal[d], Reidar G. Trønnes[a,b,h], Susan J. Webb[d], and Abigail L. Bull[a]

[a]Centre for Earth Evolution and Dynamics, University of Oslo, 0316 Oslo, Norway; [b]Centre for Advanced Study, 0271 Oslo, Norway; [c]Geodynamics, Geological Survey of Norway, 7491 Trondheim, Norway; [d]School of Geosciences, University of the Witwatersrand, WITS 2050 Johannesburg WITS 2050, South Africa; [e]Department of Earth and Environmental Sciences, University of Michigan, Ann Arbor, MI 48109; [f]Department of Geosciences, University of Houston, Houston, Texas 77204; [g]Helmholtz Centre Potsdam, GFZ German Research Centre for Geosciences, 14473 Potsdam, Germany; and [h]Natural History Museum, University of Oslo, 0318 Oslo, Norway

Earth's residual geoid is dominated by a degree-2 mode, with elevated regions above large low shear-wave velocity provinces on the core–mantle boundary beneath Africa and the Pacific. The edges of these deep mantle bodies, when projected radially to the Earth's surface, correlate with the reconstructed positions of large igneous provinces and kimberlites since Pangea formed about 320 million years ago. Using this surface-to-core–mantle boundary correlation to locate continents in longitude and a novel iterative approach for defining a paleomagnetic reference frame corrected for true polar wander, we have developed a model for absolute plate motion back to earliest Paleozoic time (540 Ma). For the Paleozoic, we have identified six phases of slow, oscillatory true polar wander during which the Earth's axis of minimum moment of inertia was similar to that of Mesozoic times. The rates of Paleozoic true polar wander (<1°/My) are compatible with those in the Mesozoic, but absolute plate velocities are, on average, twice as high. Our reconstructions generate geologically plausible scenarios, with large igneous provinces and kimberlites sourced from the margins of the large low shear-wave velocity provinces, as in Mesozoic and Cenozoic times. This absolute kinematic model suggests that a degree-2 convection mode within the Earth's mantle may have operated throughout the entire Phanerozoic.

plate reconstructions | thermochemical piles

Two equatorial, antipodal, large low shear-wave velocity provinces (Fig. 1) in the lowermost mantle (1) beneath Africa (termed Tuzo) (2) and the Pacific Ocean (Jason) are prominent in all shear-wave tomographic models (3–7) and have been argued to be related to a dominant degree-2 pattern of mantle convection that has been stable for long times (3). Most reconstructed large igneous provinces and kimberlites over the past 300 My have erupted directly above the margins of Tuzo and Jason, which we term the plume generation zones (1, 2, 5). This remarkable correlation suggests that the two deep mantle structures have been stable for at least 300 My. Stability before Pangea (before 320 Ma) is difficult to test with plate reconstructions because the paleogeography, the longitudinal positions of continents, and the estimates of true polar wander are uncertain (8). It is similarly challenging to reproduce such long-term stability in numerical models (9). However, if the correlation between the eruption sites of large igneous provinces, kimberlites, and the plume generation zones observed for the past 300 Ma has been maintained over the entire Phanerozoic (0–540 Ma), it can provide a crucial constraint for defining the longitudinal positions of continental blocks during Paleozoic time (250–540 Ma).

Here we show that a geologically reasonable kinematic model that reconstructs continents in longitude in such a way that large igneous provinces and kimberlites are positioned above the plume generation zones at the times of their formation (Fig. 2A and SI Appendix, Fig. S2) can be successfully defined for the entire Phanerozoic. This model requires that Tuzo and Jason

remain nearly stationary from the early Cambrian (540 Ma) in the large-scale convection within the Earth's mantle.

Plume Generation Zones

Previous work (1, 2, 5, 10) and numerical models (9, 11) suggest that the most likely candidates for the plume generation zones in the lower mantle are those areas that correspond to the largest lateral gradients of the shear-wave velocity directly above the core–mantle boundary. Although the distribution of plume generation zones depends on the particulars of the seismic tomography model used to define them, the differences between alternative definitions are typically small (5). Torsvik and colleagues (1) used the 1% slow-velocity contour in the lowermost layer of the mean Shear-wave tomographic model SMEAN (6) to define the plume generation zones. This contour corresponds to the steepest lateral gradients of shear-wave velocity, and 80% of reconstructed large igneous provinces of the past 300 My plot within 10° of it (Fig. 1B).

A perhaps more robust definition of the plume generation zones can be deduced from the recently published cluster analysis of five global shear-wave tomography models (7). In this work, a "voting" map was produced that described whether a geographical location was above a seismically slower-than-average velocity region in the mantle below 1,000 km depth. The voting map (Fig. 1B) shows how many of the five tomographic models agree on the classification of the data point. Within contour 5, all five tomographic models show slower-than-average
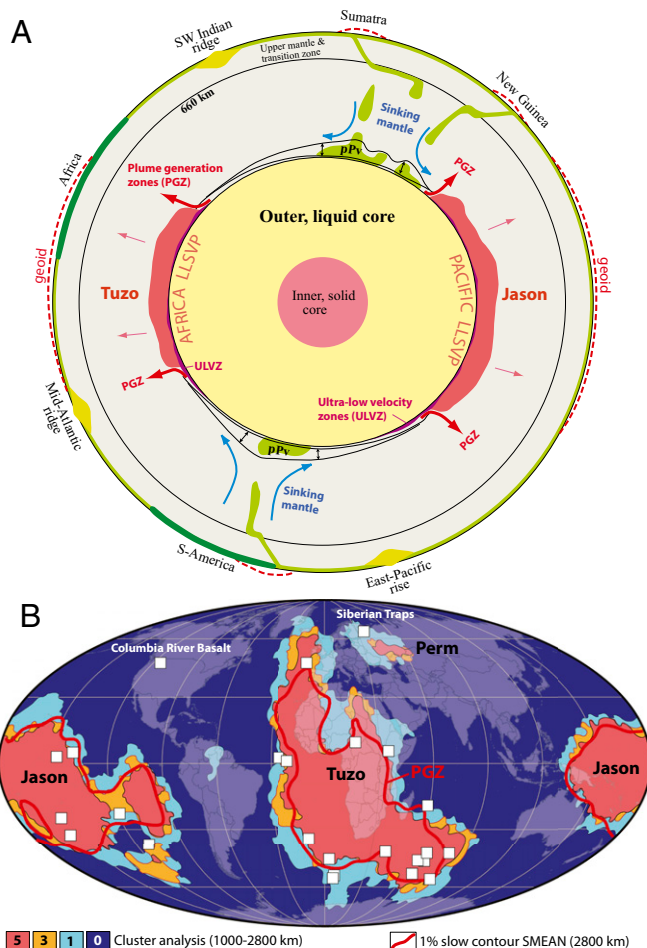
Fig. 1. (*A*) Schematic cross-section of the Earth as seen from the South Pole. The Earth's lower mantle is dominated by two antipodal large low shear-wave velocity provinces (LLSVPs) beneath Africa (Tuzo) and the Pacific (Jason). These dominate the elevated regions of the residual geoid (dashed red lines), and their margins, the plume generation zones (PGZs), are the principal source regions for large igneous provinces and kimberlites (1). The thin arrows above Tuzo and Jason are shown to indicate that the residual geoid (15) is largely a result of buoyant upwellings overlying these hot and dense mantle structures. The "pPv" (between the two lines separated by up–down arrows) indicates lenses of postperovskite (40). (*B*) Reconstructed large igneous provinces for the past 300 My (1) and the 1% slow SMEAN (6) contour (2,800 km depth) used as a proxy for the plume generation zones. Also shown are the "voting" map contours of ref. (7). Contours 5–1 (only 5, 3, and 1 are shown for clarity) define Tuzo and Jason (seismically slow regions) in addition to a smaller Perm anomaly. The Columbia River Basalt (17 My) is the only anomalous large igneous province (located above faster regions, contour 0) in these global tomographic models.

Paleozoic Plate Model

The Early Paleozoic (8) was dominated by the great continent of Gondwana. Other continents included Laurentia and Baltica (Fig. 2*A*), which fused together with the Avalonia microcontinent to form Laurussia, the second largest Paleozoic continent, after the closure of the Iapetus Ocean in the Silurian (~430 My). By the late Carboniferous (~320 My), Gondwana and Laurussia had amalgamated, forming the supercontinent of Pangea. Relative fits within Gondwana, Laurussia, and later, Pangea are reasonably well known; the sources of these reconstructions have been documented in a recent review by Torsvik and colleagues (8). In contrast, absolute Paleozoic reconstructions have remained uncertain because longitudes of continental blocks cannot be derived from paleomagnetic data (although latitudes and azimuthal orientations can). Our plate model is mainly based on apparent polar wander paths for Gondwana, Siberia, Laurentia/Baltica (Laurussia after 430 My), and their later combinations into Pangea (8). Of these paths, the Gondwana path during the Mid-Paleozoic is probably the most controversial. Euler poles were calculated from the apparent polar wander paths, and continents were reconstructed in latitude and azimuthal orientation.

Paleogeographic reconstructions relate the past configurations of continents to the Earth's spin axis (8). However, correlating the reconstructed positions of large igneous provinces and kimberlites to the plume generation zones requires reconstructions relative to the Earth's mantle. The two reference frames (paleogeographic, which we also refer to as "paleomagnetic," and the mantle frames) generally differ because over time, the solid Earth (mantle and crust) can slowly rotate with respect to the spin axis, driven by the redistribution of density heterogeneities within the solid Earth, resulting in changes of the planetary moment of inertia. This process is known as true polar wander (13). The estimates for Cenozoic and Mesozoic times (8, 14–16) suggest that the direction of true polar wander is largely controlled by the mass of the two antipodal large low shear-wave velocity provinces associated with persistent degree-2 residual geoid highs. True polar wander is therefore mainly confined to the circumpolar belt of high shear-wave velocities between Tuzo and Jason that remain close to the equator. Assuming that these deep mantle bodies have been stable over a longer time scale, we expect a similar pattern of Paleozoic polar motion, dominantly confined to the great circle passing through the geographic poles at approximately the same distance from the two large low shear-wave velocity provinces. Massive slabs, such as under North America (17), probably can contribute geoid signals of comparable magnitude, so that the pole can also move some distance toward or away from Tuzo and Jason (16).

To define the longitudes in our paleogeographic reconstructions, using the correlation between the eruption localities of large igneous provinces/kimberlites and the plume generation zones, we adopted an approach that incorporates the estimates of true polar wander that is based on the work of Steinberger and Torsvik (14) but is extended to earlier times. We compiled all dated kimberlites and large igneous provinces for the Paleozoic (*SI Appendix*, Fig. S1). For our initial model, continental longitudes in the paleomagnetic frame were defined both according to geological constraints and so that large igneous provinces or kimberlites were located directly above a plume generation zone, ignoring any possible true polar wander (and plume advection) in the Paleozoic. The next step from this idealized model was estimating true polar wander and correcting the paleogeographic reconstruction, using the obtained true polar wander rotations.

The method we used to derive the true polar wander rotations (8, 14) requires that the longitudes of the continents in the paleomagnetic frame are specified before estimating true polar wander. Because these are a priori unknown, we developed an iterative approach for defining a paleomagnetic frame, corrected

seismic velocities, whereas, for example, contour 3 outlines the area in which three of five models are in agreement. Contour 3 is similar to the 1% slow SMEAN contour (80% of large igneous provinces within 10° from both of them); however, contours 5 and 4 match the distribution of reconstructed large igneous provinces better. The cluster analysis also suggests that the ~251 Ma Siberian Traps originated from the plume generation zone of a smaller anomaly (12), now dubbed Perm (7); this anomaly is also discernible in the SMEAN model (~0.5% slow in Fig. 2*A*). For ease of comparison with earlier studies (1, 2, 5), we here use the 1% slow contour of the SMEAN model as a proxy for the plume generation zones, but we also present relevant summaries for the comparisons with the contours defined by the cluster analysis (7).
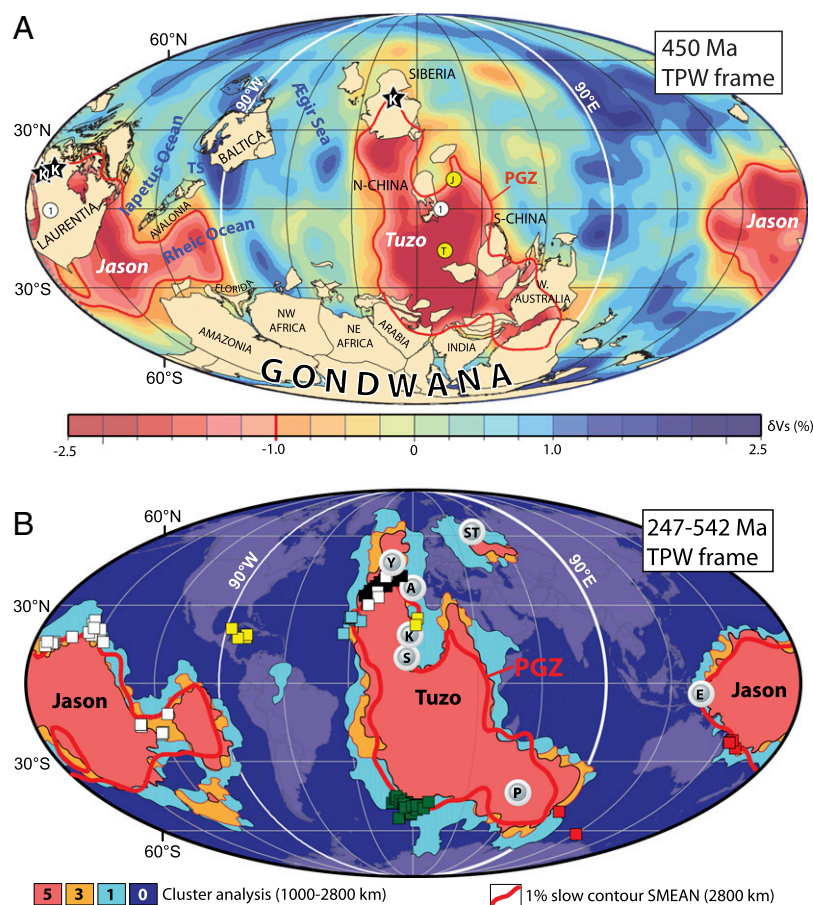
Fig. 2. (*A*), 450-My true polar wander (TPW)-corrected mantle frame reconstruction draped on the SMEAN tomographic model (6) and the plume generation zones (PGZs; 1% slow SMEAN contour). Yellow dots (marked T and J) are the center of mass (12) for Tuzo and its antipode for Jason. Open white circles (marked 1) show the preferred axis (0°N, 11°E and 169°W) for Paleozoic TPW and approximate the longitude of the minimum moment of inertia (I_{min}) axis associated with the Tuzo and Jason large low shear-wave velocity provinces, as well as the geotectonic bipolarity axis proposed by Pavoni (41). Kimberlite locations (Canada and Siberia, black stars) dated 445–455 My fall vertically above the plume generation zones. The 450 My reconstruction is only an example, and a paleogeographic cavalcade (*SI Appendix*, Figs. S7–S36), reconstruction parameters (*SI Appendix*, Table S1), and a GPlates (www.gplates.org) rotation file (GPlates Data File) are found in the *SI Appendix*. (*B*) Paleozoic large igneous provinces (annotated gray circles with white rings; 251–510 My) and kimberlites (colored and black and white squares; 247–542 My) reconstructed in a TPW-corrected reference frame to the exact eruption time (sixth and final iteration). Kimberlites are plotted with white (Laurentia), yellow (Baltica: Russia), black (Siberia), light blue (China blocks), green (Gondwana: South Africa), and red (Gondwana: Australia) colors. K, Kalkarindji (510 My, Australia); A, Altay-Sayan (400 My, Siberia); Y, Yakutsk (360 My, Siberia); S, Skagerrak (297 My, Europe); P, Panjal Traps (285 My, India/NW Himalaya; allochthonous); E, Emeishan (258 My, South China); ST, Siberian Traps (251 My). Background map as in Fig. 1*B*.

for true polar wander (*SI Appendix*, Fig. S3). Using our initial idealized Paleozoic reconstructions with no true polar wander, we computed net rotations of continents at 10 My steps, which were decomposed into component rotations along three orthogonal axes (8, 14). Axis 1 is at the equator at 11°E, which corresponds to the longitude axis of minimum moment of inertia of Tuzo and Jason (Fig. 2*A*). Episodes of coherent rotations about this axis were interpreted as a true polar wander signal (i.e., we assume that a dominant contribution from the stable large low shear-wave velocity provinces to the overall moment of inertia of the Earth stabilizes the orientation of the true polar wander axis over geologic time). Because the true polar wander corrections would generally degrade the large igneous province and kimberlite fits to the plume generation zones (*SI Appendix*, Fig. S3), the longitudes in the paleomagnetic frame were then redefined to produce an optimal fit after the true polar wander correction. This produced the second approximation for the longitude-calibrated paleomagnetic frame. The entire procedure of true polar wander analysis and longitude refinements was repeated six times until no further improvement was observed in the true polar wander-corrected frame. Our final iterations yielded six episodes

(5–10 in Fig. 3*A*) of Paleozoic true polar wander along a great circle around an equatorial axis at 11°E; this iterative procedure generates two sets of Paleozoic reconstructions: one that describes configurations of continents relative to the spin axis (paleogeography) and one in which paleogeographic reconstructions were corrected for true polar wander (Fig. 2*A*), describing plate motions relative to the Earth's mantle (*SI Appendix*, Figs. S7–S36). As an example of the latter, we show a 450 Ma reconstruction at a time when the continents were spread over a large part of the globe (Fig. 2*A*). At this time, the Iapetus Ocean separated Baltica and Avalonia from Laurentia, which itself was separated from Gondwana by the wide Rheic Ocean.

Source Regions for Paleozoic Large Igneous Provinces and Kimberlites

In our final model (*SI Appendix*, Table S1), North American and Russian (Baltican) kimberlites were sourced from the Jason plume generation zone in the early-mid Paleozoic, whereas the Late Paleozoic (~290–250 Ma) kimberlites were sourced from the Tuzo plume generation zone (*SI Appendix*, Figs. S7–S36). Conversely, Cambrian large igneous provinces and kimberlites
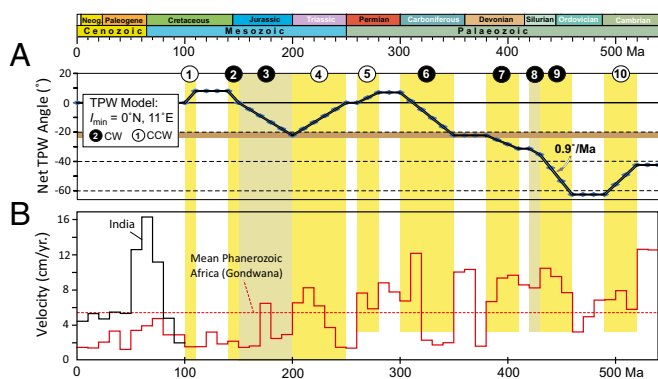
Fig. 3. (*A*) We model 10 Phanerozoic phases of clockwise (CW) and counter clockwise (CCW) rotations (TPW, true polar wander) around 0°N, 11°E: (1) 110–100 My: +8°; (2) 150–140 My: −8°; (3) 200–150 My: −22°; (4) 250–200 My: +22°; (5) 280–260 My: +7°; (6) 350–300 My: −29°; (7) 410–380 My: −9°; (8) 430–420 My: −4°; (9) 460–430 My: −27°; (10) 520–490 My: +20°. TPW phases 1–4 updated from refs. 8 and 14. The brown belt corresponds to a pole location near the I_{max} axis of both large low shear-wave velocity provinces (15). (*B*) Phanerozoic plate velocities for a central location in Africa/Gondwana (8°N, 19°E), based on Paleozoic (this study) and Mesozoic (8) TPW-corrected reference frames and a moving hotspot frame after 125 Ma (16). Average velocities are higher than for Mesozoic–Cenozoic times, but for comparison, we also show plate velocities for a central location in India (22°N, 76°E) for the past 100 My (16). Between 70 and 60 Ma, India shows a velocity burst of more than 16 cm/y.

from South Africa were sourced by the Tuzo plume generation zone, and a short-lived kimberlite event (380–370 Ma) in Australia was sourced by the Jason plume generation zone. All large igneous provinces and kimberlites from Siberia and China come from the Tuzo and Perm plume generation zone except the Emeishan large igneous province in South China (5), sourced from the Jason plume generation zone at 258 Ma. Whenever possible, large igneous provinces and kimberlites were modeled to be located directly above the plume generation zones, but some positions were selected as a compromise between multiple kimberlite and large igneous province sites. The largest deviation from a plume generation zone was observed for ~400 Ma Russian kimberlites (yellow squares in Fig. 2*B*) because we fitted similar-aged kimberlites in North America to the Jason plume generation zone. Both areas were part of Laurussia, and our choice maintains more credible plate velocities for Laurussia (*SI Appendix*, Fig. S5A). The Panjal Traps (allochtonous) and the Siberian Traps were not modeled (forced) to be located directly above the margins of Tuzo.

In the true polar wander-corrected frame, five of seven Paleozoic large igneous provinces plot within 5° of the plume generation zones, and one (Panjal Traps) plots 11.2° away. Of 231 kimberlites, 98% plot within 10° of a plume generation zone (Fig. 2*B* and *SI Appendix*, Table S2). Although our longitude fitting method used the 1% slow SMEAN contour (6) as a proxy for the plume generation zones, the statistical correlation is similar and even improved compared with the seismic voting map contours (7). As an example, all large igneous provinces (including the Siberian Traps) plot within 10° of contour 4 (Fig. 2*B* and *SI Appendix*, Table S2).

Plate Velocities and Rates of True Polar Wander

Our Paleozoic model is consistent with the geological surface record of the opening and closure of the main Paleozoic Oceans. However, the developing Iapetus Ocean in Cambrian times is uncertain because of poor or absent data (notably from Baltica). Current Cambrian paleogeography and plate velocity estimates should therefore be viewed with caution.

Plate velocities calculated for central locations in Gondwana, Laurentia, Baltica, their later amalgamation into Laurussia, and Siberia are below 20 cm/y (*SI Appendix*, Figs. S4 and S5), but the average velocities are about twice as high (Fig. 3*B*) as those in Mesozoic and Cenozoic times (18, 19). The most extreme velocities in our model are seen for parts of peri-Gondwana and, notably, Australia (*SI Appendix*, Fig. S5B). Angular rotations are also high, with Gondwana rotating strongly counterclockwise in the Cambrian and clockwise in Late Ordovician/Silurian times. True polar wander corrections led to smaller/slower angular rotations, but they are still pronounced in our Paleozoic model. Higher-than-normal plate velocities (Fig. 3*B*) may arise from our longitude calibration method or a combination of poor paleomagnetic data (recording north–south velocity only) and inadequate true polar wander corrections. We model 10 phases of slow (≤0.9°/My; ≤10 cm/y) and oscillatory true polar wander for the entire Phanerozoic, but net true polar wander rotations peak at −62° in the Ordovician (Fig. 3*A*). True polar wander estimates before the Carboniferous (360–540 My), however, should be treated with caution because the continental masses were dominantly in the southern hemisphere at polar latitudes (*SI Appendix*, Fig. S6). It is, therefore, difficult to differentiate between north–south plate motion and true polar wander without assuming a specific location of the axis of minimal moment of inertia, I_{min}. For example, Mitchell and colleagues (20) postulated that I_{min} was 90° further to the east during much of the Paleozoic, migrating westward to its present position between 370 and 260 Ma. Their reconstructions, using very different assumptions and "locking" Australia near the equator at 110°E (assumed I_{min} longitude) from 500–390 Ma, may at times show some similarities with ours, but their model features fast plate velocities (except for Australia), and overall, the reconstructed large igneous provinces and kimberlites are uncorrelated with the margins of Tuzo and Jason (only 30% within 10° from their margins).

Before true polar wander correction, absolute plate velocities for a central location in Africa show velocity spikes (~15 cm/y) in the Late Cambrian, Silurian, and Late Carboniferous (*SI Appendix*, Fig. S4). The latter, however, is linked to north–south motion based on paleomagnetic inclination data alone and, thus, is not a result of longitude calibrations. African (Gondwanan) plate velocities are reduced after true polar wander correction, averaging 7.3 cm/y, and only the Late Carboniferous (320–310 Ma) spike, reduced to ~12 cm/y, remains (Fig. 3*B* and *SI Appendix*, Fig. S4). For a central location in North America, we note in our true polar wander-corrected reconstructions a Late Silurian–Early Devonian (420–410 Ma) velocity spike (~17 cm/y; *SI Appendix*, Fig. S5A) shortly after the formation of Laurussia (Baltica–Avalonia merging with Laurentia); this peak also occurs in the north–south motion of Laurussia (~10 cm/y in North America) and is therefore not an artifact of longitude calibrations. Laurussia must have drifted eastward from the Late Devonian to source Late Paleozoic kimberlites, mostly Canadian, and the Skagerrak Centered large igneous province (~297 Ma) from the Tuzo PGZ. The modeled change from the Jason to the Tuzo plume generation zone requires plate velocities of 10–17 cm/y (370–310 Ma; *SI Appendix*, Fig. S5A). These modeled velocities are certainly higher than those that would be normally expected for large continental blocks, except for the high velocities recorded for India in Late Mesozoic/Early Cenozoic times (Fig. 3*B*).

Most large igneous provinces and kimberlites plot within 10° of a plume generation zone in our model (Fig. 2*B* and *SI Appendix*, Table S2). We note that for more recent times after Pangea assembly, when plate motions are better constrained, we are not able to fit all large igneous provinces and kimberlites above the margins of Tuzo and Jason, particularly Late Cretaceous and Early Tertiary kimberlites in North America (1), the Columbia River Basalt, and Siberian Traps (Fig. 1*B*). Likewise, it is possible

that some of the earlier large igneous provinces and kimberlites we are fitting here do not originate directly above these margins. Relaxing this constraint to fit most large igneous provinces and kimberlites precisely over the margins of Tuzo and Jason could yield plate reconstructions with slower plate motions. However, we prefer not to take such an approach here because it would introduce arbitrariness.

Another potential source of uncertainty in our reconstructions is the geometry of Pangea in the Late Paleozoic. We model an Early Carboniferous Pangea B type configuration (Laurussia located "west" of Gondwana; *SI Appendix*, Figs. S25–S29), evolving into a Pangea A-type configuration at 320 Ma (19, 21). Conversely, Muttoni and colleagues (22) maintain a Pangea B fit between ~300 and 270 Ma, with Laurussia located 5,000 km "west" of Gondwana (*SI Appendix*, Fig. S37). There are few large igneous provinces, and kimberlites erupted between 320 and 270 Ma, but they do show a better fit to a plume generation zone in a Pangea A configuration. However, a slightly younger transition from Pangea B to A could reduce the Carboniferous velocities for Laurussia.

Sources of True Polar Wander

Adding dense material in the upper mantle at intermediate to high latitudes must be a prime candidate for causing true polar wander, and geoid kernel modeling (15, 23) suggests that the maximum effect is achieved 30–40 My after subduction initiation, when slabs arrive in the transition zone (Fig. 4A). The effect of slabs in the lower mantle is expected to be smaller, because thermal expansivity of mantle material becomes smaller with depth. However, this may be partly compensated for by a larger amount of slabs in the lower mantle as a result of lower sinking speeds. The exact shape of geoid kernels depends on viscosity structure and phase boundary parameters (Clapeyron slope, density jump, thermal expansivity); however, a degree-2 kernel that is positive in the upper part of the mantle and negative in its lower part is a robust feature of mantle models that successfully reproduce large-scale features of the geoid (24–26). Hence, we expect that the intermediate- to high-latitude subduction would preferentially induce true polar wander so that subduction zones shift toward the equator, possibly with some time delay (Fig. 4A).

Between 520 and 490 My, we find counter-clockwise true polar wander rotation, which could be related to subduction primarily occurring in the lower right quadrant of the maps shown in the top panels of *SI Appendix*, Figs. S9–S12, during those or somewhat earlier times. For the period 460–300 Ma, a clockwise rotation corresponds to subduction occurring in the lower left quadrant (*SI Appendix*, Figs. S15–S29, *Upper*) related to the closure of the Iapetus and Rheic oceans (Fig. 2A). In particular, extensive intermediate- to high-latitude peri-Gondwanan subduction in Late Cambrian–Early Ordovician times (Fig. 4B) provides a simple explanation for the "high" rates of true polar wander between 460 and 430 Ma (0.9°/My; Fig. 3). However, a systematic study of how subduction zone locations relate to true polar wander (27, 28) would require full plate reconstructions (not just locations of continents) and is not attempted here.

The overall true polar wander signal dating from 540 My can be interpreted as oscillatory swings approximately around the same axis (0°N, 11°E), centered on a rotation angle of ~22° (Fig. 3), which corresponds to a pole location near the axis of maximum moment of inertia for the combined masses of Tuzo and Jason. This pole location would be expected if the Earth's moment of inertia were defined by the contribution from Tuzo and Jason alone (15). Deviations from that location can be explained by subduction (15), but because of persistent triaxial shape or lithospheric elasticity (27), the pole would have a tendency to return to its original location after the termination of subduction. This mechanism can complement the true polar wander forced

Fig. 4. (A) Geoid kernel (Model-I in ref. 15) and the corresponding age–depth relationship for sinking slabs (red numbers). We also show the age–depth relationship (black numbers) suggested by van der Meer and colleagues (42) for Mesozoic–Cenozoic times. Geoid kernels are for total (thermal plus chemical) density anomaly and include the effect of density anomalies themselves and displaced boundaries (surface and core–mantle boundary). Positive geoid associated with large low shear-wave velocity provinces hence implies that the effect of the thermal anomaly, partly in the mantle above and in the form of rising plumes, overcompensates any effect of compositionally heavier material. The transition zone (410–660 km) is shown in dark gray shading. (B) The south-pole (SP) of the paleomagnetic frame was located in north Africa in the Late Cambrian (~500 My). Peri-Gondwana subduction is shown as teeth on thin lines and marks trench locations in the paleomagnetic reference frame. The teeth are in the upper plate and indicate the polarity of subduction. Outboard Avalonia, for instance, was adjacent to subduction at high latitudes at 500 Ma (red line and teeth). This pattern of high-latitude subduction continued during the Ordovician but shifted toward lower latitudes (<60°S) by the Early Silurian (~440 My). The trench length, and hence the volume of dense material sinking into the upper mantle, were also reduced during the Ordovician.

by ongoing subduction, providing an explanation for its oscillatory nature in more recent times (16).

Long-Term Stability of Deep Mantle Structures

The two antipodal large low shear-wave velocity provinces, Tuzo and Jason, must impose strong and long-lived control on Earth's thermal, magmatic, magnetic, and rotational dynamics; they may organize the global mantle flow (3, 29), and their edges are favorable sites for the initiation of deep mantle plumes (9–12). A thermochemical constitution of Tuzo and Jason is supported by geochemical observations of multiple chemical reservoirs at depth, strong seismic contrasts, an anticorrelation of shear-wave velocity to bulk sound velocity, and increased density in these regions (4, 30–33). Although a few recent studies argued that all these observations could be explained by thermal anomalies alone (e.g., ref. 34), the long-term stability of Tuzo and Jason is highly unlikely for purely thermal features.

Whereas recycled oceanic crust of basaltic composition may be a candidate material for at least part of Tuzo and Jason, peridotitic materials enriched in iron and perovskite provide a better fit to the seismic properties (35). Magmatic segregations of Fe-rich peridotitic or komatiitic materials could most easily have formed during early magma ocean crystallization or shortly afterward (36–39). Our reconstructions, in which Tuzo and Jason appear to have been stable throughout the Phanerozoic, suggest

that a very early origin of these deep mantle structures is a viable hypothesis, and our approach can potentially be paleomagnetically extended to the assembly of Rodinia, about 1 billion years ago.

We would like to stress that the Paleozoic model developed here is a kinematic model for the continents and that the next step in improving it will be developing a global model for the entire lithosphere (including synthetic oceanic lithosphere). This is challenging for the Paleozoic (19) but is essential for assessing whether our model is tectonically and geodynamically plausible, testing the potential longevity of Tuzo and Jason through numerical modeling and comparing the modeled estimates of true polar wander because of subduction with those inferred from comparisons of plate reconstructions in the mantle and paleomagnetic reference frames.

1. Torsvik TH, Burke K, Steinberger B, Webb SJ, Ashwal LD (2010) Diamonds sampled by plumes from the core-mantle boundary. *Nature* 466(7304):352–355.
2. Burke K (2011) Plate Tectonics, the Wilson Cycle, and Mantle Plumes: Geodynamics from the Top. *Ann Rev Earth Planet Sci* 39:1–29.
3. Dziewonski AM, Lekic V, Romanowicz BA (2010) Mantle Anchor Structure: An argument for bottom up tectonics. *Earth Planet Sci Lett* 299:69–79.
4. Lay T, Garnero EJ (2011) Deep Mantle Seismic Modeling and Imaging. *Annu Rev Earth Planet Sci* 39:91–123.
5. Torsvik TH, Steinberger B, Cocks LRM, Burke K (2008) Longitude: Linking Earth's ancient surface to its deep interior. *Earth Planet Sci Lett* 276:273–283.
6. Becker TW, Boschi L (2002) A comparison of tomographic and geodynamic mantle models. *Geochem Geophys Geosyst* 3:GC000168.
7. Lekic V, Cottar S, Dziewonski A, Romanowicz B (2012) Cluster analysis of global lower mantle tomography: A new class of structure and implications for chemical heterogeneity. *Earth Planet Sci Lett* 357:68–77.
8. Torsvik TH, et al. (2012) Phanerozoic polar wander, paleogeography and dynamics. *Earth Sci Rev* 114:325–368.
9. Tan E, Leng W, Zhong S, Gurnis M (2011) On the location of plumes and mobility of thermo-chemical structures with high bulk modulus in the 3-D compressible mantle. *Geochem Geophys Geosyst* 12:Q07005.
10. Thorne MS, Garnero EJ, Grand S (2004) Geographic correlation between hot spots and deep mantle lateral shear-wave velocity gradients. *Phys Earth Planet Inter* 146:47–63.
11. Steinberger B, Torsvik TH (2012) A geodynamic model of plumes from the margins of Large Low Shear Velocity Provinces. *Geochem Geophys Geosyst* 13:GC003808.
12. Burke K, Steinberger B, Torsvik TH, Smethurst MA (2008) Plume Generation Zones at the margins of Large Low Shear Velocity Provinces on the Core-Mantle Boundary. *Earth Planet Sci Lett* 265:49–60.
13. Goldreich P, Toomre A (1969) Some remarks on polar wandering. *J Geophys Res* 74:2555–2569.
14. Steinberger B, Torsvik TH (2008) Absolute plate motions and true polar wander in the absence of hotspot tracks. *Nature* 452(7187):620–623.
15. Steinberger B, Torsvik TH (2010) Toward an explanation for the present and past locations of the poles. *Geochem Geophys Geosyst* 11:GC002889.
16. Doubrovine PV, Steinberger B, Torsvik TH (2012) Absolute plate motions in a reference frame defined by moving hotspots in the Pacific, Atlantic and Indian oceans. *J Geophys Res* 117:B09101.
17. Sigloch K, Mihalynuk MG (2013) Intra-oceanic subduction shaped the assembly of Cordilleran North America. *Nature* 496(7443):50–56.
18. Gurnis M, Torsvik TH (1994) Rapid drift of large continents during the late Precambrian and Palaeozoic: Palaeomagnetic constraints and dynamic models. *Geology* 22:1023–1026.
19. Domeier M, Torsvik TH (2014) Focus Review Paper: Plate kinematics of the Late Paleozoic. *Geoscience Frontiers* 5:303–350.
20. Mitchell RN, Kilian TM, Evans DAD (2012) Supercontinent cycles and the calculation of absolute palaeolongitude in deep time. *Nature* 482(7384):208–211.
21. Domeier M, Van der Voo R, Torsvik TH (2012) Review Article: Paleomagnetism and Pangea: The Road to reconciliation. *Tectonophysics* 514-517:14–43.
22. Muttoni G, et al. (2009) Opening of the Neo-Tethys Ocean and the Pangea B to Pangea A transformation during the Permian. *GeoArabia* 14:17–48.
23. Hager BH (1984) Subducted slabs and the geoid: Constraints on mantle rheology and flow. *J Geophys Res* 89:6003–6015.
24. Hager BH, Richards MS (1989) Seismic Tomography and Mantle Circulation. *Philosoph Trans R Soc Lond Series A* 328:309–327.
25. Steinberger B, Calderwood A (2006) Models of large-scale viscous flow in the Earth's mantle with constraints from mineral physics and surface observations. *Geophys J Int* 167:1461–1481.
26. Steinberger B, Holme R (2008) Mantle flow models with core-mantle boundary constraints and chemical heterogeneities in the lowermost mantle. *J Geophys Res* 113:B05403.
27. Creveling JR, Mitrovica JX, Chan N-H, Latychev K, Matsuyama I (2012) Mechanisms for oscillatory true polar wander. *Nature* 491(7423):244–248.
28. Evans DAD (2003) True polar wander and supercontinents. *Tectonophysics* 362:303–320.
29. Conrad CP, Steinberger B, Torsvik TH (2013) Stability of active mantle upwelling revealed by net characteristics of plate tectonics. *Nature* 498(7455):479–482.
30. Hofman AW (1997) Mantle geochemistry: The message from oceanic volcanism. *Nature* 385:219–229.
31. Wang Y, Wen L (2004) Mapping the geometry and geographic distribution of a very low velocity province at the base of the Earth's mantle. *J Geophys Res* 109:B10305.
32. Ishii M, Tromp J (1999) Normal-mode and free-Air gravity constraints on lateral variations in velocity and density of Earth's mantle. *Science* 285(5431):1231–1236.
33. Hernlund JW, Houser C (2008) On the statistical distribution of seismic velocities in Earth's deep mantle. *Earth Planet Sci Lett* 265:423–437.
34. Davies DR, et al. (2012) Reconciling dynamic and seismic models of Earth's lower mantle: The dominant role of thermal heterogeneity. *Earth Planet Sci Lett* 353:253–269.
35. Deschamps F, Cobden L, Tackley PJ (2012) The primitive nature of large low shear wave velocity provinces. *Earth Planet Sci Lett* 349-350:198–208.
36. Labrosse S, Hernlund JW, Coltice N (2007) A crystallizing dense magma ocean at the base of the Earth's mantle. *Nature* 450(7171):866–869.
37. Stixrude L, de Koker N, Sun N, Mookherjee M, Karki BB (2009) Thermodynamics of silicate liquids in the deep Earth. *Earth Planet Sci Lett* 278:226–232.
38. Lee CT, et al. (2010) Upside-down differentiation and generation of a 'primordial' lower mantle. *Nature* 463(7283):930–933.
39. Liebske C, Frost DJ (2012) Melting phase relations in the MgO–MgSiO$_3$ system between 16 and 26 GPa: Implications for melting in Earth's deep interior. *Earth Planet Sci Lett* 345-348:159–170.
40. Trønnes RG (2010) Structure, mineralogy and dynamics of the lowermost mantle. *Min Petrol* 99:243–261.
41. Pavoni N (1985) Pacific/anti - Pacific bipolarity in the structure of the Earth's mantle. *Eos Trans AGU* 66:497.
42. van der Meer D, Spakman W, van Hinsbergen DJJ, Amaru ML, Torsvik TH (2010) Absolute plate motions since the Permian inferred from lower mantle slab remnants. *Nat Geosci* 3:36–40.

Torsvik et al.